ACS APPLIED MATERIALS & INTERFACES

Research Article

www.acsami.org

Strong Highly Anisotropic Magnetocellulose Nanocomposite Films Made by Chemical Peeling and In Situ Welding at the Interface Using an Ionic Liquid

Mahdi Mashkour,*[,†] Mehdi Tajvidi,[‡] Fumiko Kimura,[§] Hossein Yousefi,[†] and Tsunehisa Kimura[§]

[†]Department of Wood Engineering and Technology, Faculty of Wood and Paper Engineering, Gorgan University of Agricultural Sciences and Natural Resources, Gorgan 49189-43464, Iran

[‡]School of Forest Resources, University of Maine, Orono, Maine 04469, United States

[§]Fibrous Biomaterials Laboratory, Division of Forest and Biomaterials Science, Graduate School of Agriculture, Kyoto University, Kyoto 606-8502, Japan

ABSTRACT: Magnetic cellulosic papers have attracted considerable interest because of their potential applications in advanced information storage devices and security papers. However, these papers are often mechanically weak and structurally and magnetically in-plane isotropic, which restrict their applications especially where stronger anisotropic materials are required. Here, we report the production and properties of a strong anisotropic superparamagnetic cellulose nanocomposite (ASPCNC) film with high in-plane anisotropy prepared using ionic liquid (IL)-based peeling and in situ welding processes. Field-emission scanning electron microscopy, energy-dispersive X-ray analysis, X-ray diffraction, attenuated total reflection Fourier transform infrared spectroscopy, atomic force microscopy, magnetic force microscopy, and vibrating sample magnetometry were used to characterize the produced nanocomposite films. Mechanical and magnetic in-plane anisotropy were measured, and their relationships with the structural properties were determined. Tensile failure behavior of the ASPCNCs was also compared with predictions from Hankinson's failure model. The results show highly significant relationships between increasing partial dissolution time as the development index of the IL-based peeling and in situ welding procedures and improvements in the mechanical properties and structural, mechanical, and magnetic in-plane anisotropy of the ASPCNCs. Reasons behind these observations are extensively discussed.

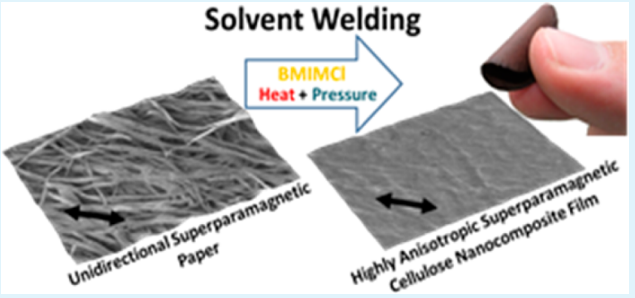

KEYWORDS: *Magneto-cellulose nanocomposite film, ionic liquid-based peeling, in-situ welding, interface, superparamagnetic, in-plane anisotropy*

INTRODUCTION

Magnetic cellulosic papers (MCPs) present high potential applications for fabricating magnetic information storage devices, security cards, electromagnetic shields, and other specialty end uses,[1−6] but the existence of magnetic nanoparticles in the structure of the MCPs dramatically decreases the interfiber bonds, leading to low mechanical properties, which limits the growth of MCPs as advanced materials.[3−5] Recently, our research group reported the successful fabrication of superparamagnetic cellulosic papers with a unidirectionally aligned structure using a simple laboratory-scale magnetic-forming machine (Magform) equipped with a weak permanent magnet (0.18 T).[7] Quick and anisotropic responses to weak modulated external magnetic fields are important parameters in the production of magnetic microswitches and highly sensitive magnetic microsensors.[8] Here, we report the fabrication of a new generation of magnetocellulose nanocomposite films that are flexible and exhibit highly anisotropic and, at the same time, strong structural, mechanical, and magnetic properties prepared by an ionic liquid (IL)-based peeling and in situ welding technique. The term "ionic-liquid-based peeling" or its abbreviated form (IL-BP), which is used here, refers to removal of the magnetic nanoparticles from the surface of covered cellulose long fibers by time-controlled direct exposure to a proper solvent, and the term "ionic-liquid-based in situ welding" (IL-BISW) refers to the binding of two or more individual peeled-off cellulosic fibers together and formation of a solid interphase between them. In the context of this paper, these two processes take place together, starting with the IL-BP process and concluding with the IL-BISW process. For this reason, the collective term "IL-Process" is used to refer to both processes. Individual names are used when a particular section of the process is discussed.

ILs, well-known as green solvents, are one of the latest developed cellulose solvent systems.[9−15] The word "green" refers to the properties of ILs, including their recyclability and reusability and lack of volatile organic compounds.[9,10,13,15] Cellulose fibers can be partially dissolved in a proper solvent at

Published: May 12, 2014

   dx.doi.org/10.1021/am500709t | *ACS Appl. Mater. Interfaces* 2014, 6, 8165−8172

controlled dissolution times. The partially dissolved/resolidified cellulose fibers can then tightly bind together because of the formation of noncrystalline cellulose as the bonding interphase between them, leading to the formation of fully biodegradable all-cellulose composites.[11,13,16−22] These all-cellulose composites are composed of noncrystalline cellulose and undissolved cellulose I_β as the matrix and reinforcing phases, respectively.[11,19,21] The resulting all-cellulose composite exhibits higher mechanical properties than the starting cellulose fiber sheet.[11,13,17,19,20] If the cellulose fibers can be unidirectionally aligned during processing, an additional advantage in terms of mechanical properties and anisotropy can be achieved.[18] The all-cellulosic-based magnetopolymer nanocomposite film reported here boasts anisotropic magnetic actuation in conjunction with highly improved anisotropic stiffness, strength, and flexibility in addition to other promising advantages of cellulose as the most abundant biobased and biocompatible polymer. As a result, the anisotropic superparamagnetic cellulose nanocomposite (ASPCNC) will be a promising candidate as a high potential material when having all mentioned properties important to making a special advanced microdevice such as magnetic gating valves in microfluidic control systems, magnetic beads in bioassays, high-performance memory devices, security cards, electromagnetic shields, and magnetic sensitive components for designing flying microrobots is desired.[4,5,23−27] It is predictable that many other potential applications will be found for this new class of magnetopolymer nanocomposites in the future.

EXPERIMENTAL SECTION

Fabrication Process. Fabricating superparamagnetic cellulose fibers and forming the starting unidirectional superparamagnetic mats (USPMs) were carried out in the same manner as fully described elsewhere by the authors.[7] Scheme 1 shows the schematic route to making final nanocomposite films. In summary, magnetite nanoparticles were synthesized in situ and precipitated on natural cellulose fibers. The superparamagnetic fibers were then suspended in a water medium, followed by being subjected to a weak permanent magnetic field (~0.18 T) while being aligned during deposition on the forming net. The obtained oriented superparamagnetic mats were then cold-pressed and oven-dried under pressure. To apply the IL-based in situ welding technique to the fibrous components, 1-butyl-3-methylimidazolium chloride (BMIMCl) was used as one of the most widely used ILs for cellulose dissolution. The fabricated mats and solvent were both oven-dried at 103 °C for 24 h, and then the IL-BP was carefully performed in an oven at a constant temperature of 85 °C. Three levels of partial dissolution time (30, 45, and 60 min) were selected as the progress indicator of the IL-Process to evaluate the effect of IL treatment on the final properties of the resulting nanocomposite films. Preliminary trials showed that the IL-BP progress had a strong negative effect on the unidirectional alignment and in-plane anisotropy of the nanocomposite films. It seemed that, during the IL-BP, the cellulose fiber components freely swelled, and transformation, movement, and slippage of the fibers past each other led to the loss of alignment. To eliminate the negative effects of these phenomena, the partial dissolution process and subsequent resolidification were carried out, while the oriented superparamagnetic mats were tightly clipped between a pair of glass slides. At the end of the designated dissolution times, the clamped samples were removed from the oven and allowed to cool to ambient temperature for 1 h. The partially dissolved samples were then rinsed in methanol and a distilled water bath (each for 48 h), successively. After rinsing, the wet films were oven-dried at 75 °C for 48 h, resulting in a self-reinforced unidirectional superparamagnetic cellulose nanocomposite. Hereafter, the produced anisotropic superparamagnetic cellulose nanocomposite films are referred to as "ASPCNC". The ASPCNCs were conditioned at room temperature and humidity for 72 h prior to each test.

Scheme 1. Schematic Representation of the Fabrication Process of the ASPCNC

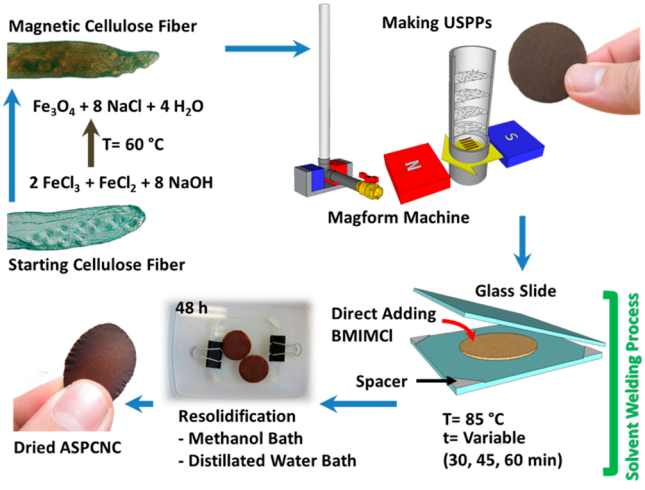

Characterization. The platinum-coated specimens were observed with a field-emission scanning electron microscope (Hitachi S-4800, Hitachi Science System Ltd., Japan), operating at an accelerating voltage of 1.5 kV.

X-ray diffraction (XRD) measurements were performed using a MAC Science Dip 2020 diffractometer (MAC Science, Japan) in the 2θ range of 5−70°. The specimens were irradiated by Cu Kα radiation at 45 kV and 84 mA in a direction perpendicular to the specimen surface. The crystallinity index (CrI) was evaluated using the following equation:[28]

$$\mathrm{CrI} = 100(I_{200} - I_{\mathrm{am}})/I_{200} \quad (1)$$

where I_{200} is the diffraction intensity assigned to the (200) reflection of cellulose I_β, which is typically in the range 2θ = 21−23°. I_{am} is the intensity measured at 2θ = 18°, where the maximum occurs in a diffractogram for noncrystalline cellulose. The crystallite size of cellulose was estimated by Scherrer's equation:[28]

$$D = \lambda/\beta \cos\theta \quad (2)$$

where D is the crystallite size, λ is the X-ray wavelength (0.15418 nm), θ is the diffraction angle for the (200) plane, and β is the corrected integral width.

The thermal stability of the samples was evaluated using thermogravimetric analysis (TGA) equipment (Hi-Res TGA 2950, TA, USA) at a heating rate of 5 °C/min from 20 to 550 °C in an inert nitrogen atmosphere to avoid premature degradation.

Energy-dispersive X-ray spectroscopy (EDS) was performed on an EDAX instrument (Genesis XM2, USA) set on the FE-SEM S-4800 microscope. The accelerating voltage and working distance were 20 kV and 15 mm, respectively.

Scanning probe microscopy (SPM) analysis was done using a Shimadzu SPM-9600 microscope (Shimadzu Co., Kyoto, Japan). Atomic force microscopy (AFM) and magnetic force microscopy (MFM) micrographs were performed, and corresponding micrographs were obtained from a scan area of 10 × 10 μm^2.

Static tensile tests were carried out using a FGP-50 tensiometer (Nidec-Shimpo Corp., Japan). The nominal dimensions of the tensile samples were 20 and 5 mm in length and width, respectively. The distance between clamps and extension rate were 10 mm and 10 mm/min, respectively.

Magnetic measurements were carried out using a vibrating sample magnetometer (made in Kashan University, Iran) at room temperature and a maximum applied field of 10 kOe.

To investigate the effects of the IL-Process on the magnetic in-plane anisotropy of the ASPCNCs, samples were cut into the same size circular slabs and then the prepared slabs were tested in an innovative

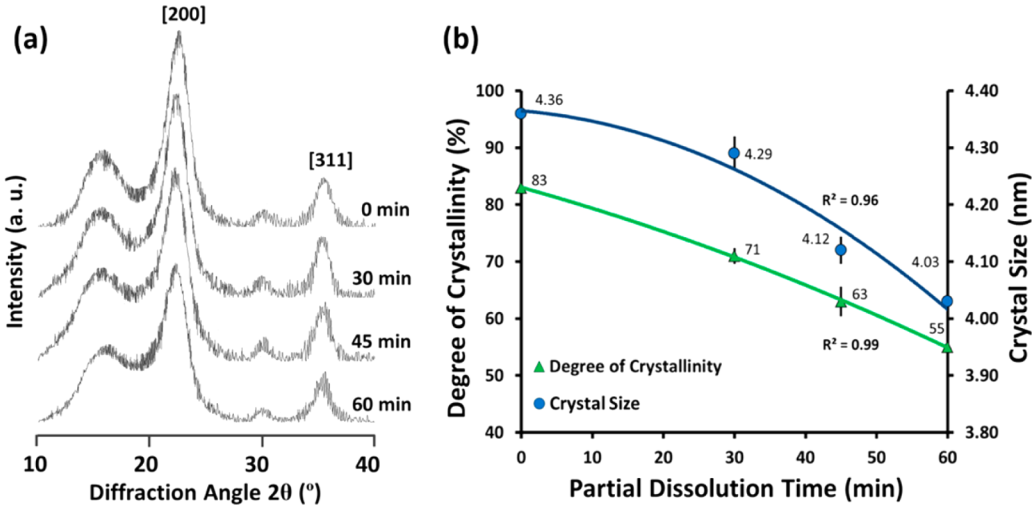

Figure 1. (a) XRD patterns of the superparamagnetic cellulose fiber mat and ASPCNCs at different partial dissolution times up to 60 min. (b) Relationships between the partial dissolution time and changes in the crystallinity and crystal size of cellulose for the ASPCNCs.

simple test setup. To compare the in-plane magnetic anisotropy of specimens, the time required to align parallel to the direction of the applied external magnetic field and reach a stable position, after being released from the direction perpendicular to the magnetic field, was measured and recorded for each sample. Shorter realignment times were considered as an indicator of better response.

RESULTS AND DISCUSSION

Figure 1 shows (a) the XRD profiles of the nanocomposite films prepared at different dissolution times and (b) their corresponding cellulose crystallinity and crystal size. The results indicated that, with increasing partial dissolution time from 0 to 60 min, the cellulose crystal size and percent crystallinity decreased from 4.36 to 4.03 nm and from 83% to 55%, respectively. Evaluation of the obtained XRD patterns showed no significant shift of the (200) peak to the left, with increasing partial dissolution time indicating that the dissolved cellulose type I_β was mostly restructured to amorphous cellulose after resolidification. Therefore, the final nanocomposite films were composed of different ratios of the two main structures: the first reinforcement or partially dissolved initial long cellulose fibers (cellulose type I_β) and the second restructured cellulose type I_β to the amorphous structure, as the binding interphase or matrix.

Parts a and b of Figure 2 show field-emission scanning electron microscopy (FE-SEM) micrographs from the surface of the starting USPMs before the IL-Process and the fine in situ synthesized magnetite nanoparticles precipitated on the surface of long cellulose fiber components. The diameter of the magnetite nanoparticles was 6 nm on average, which was well below the critical magnetite particle size, rendering the mats superparamagnetic.[7] Parts c and d of Figure 2 show FE-SEM micrographs obtained from cross sections of the produced ASPCNCs parallel to the fibrous components. These micrographs indicate that, with increasing partial dissolution time to 60 min, the porous structure of the initial USPMs changed to a compact bed containing the least amount of porosity. During the partial dissolution phase, dissolved cellulose flows between the fibrous components and fills the structural porosities. After resolidification, the resultant amorphous cellulose tightly bonds together the remaining partially dissolved initial long cellulose fibers. On the other hand, as Figure 2d clearly illustrates,

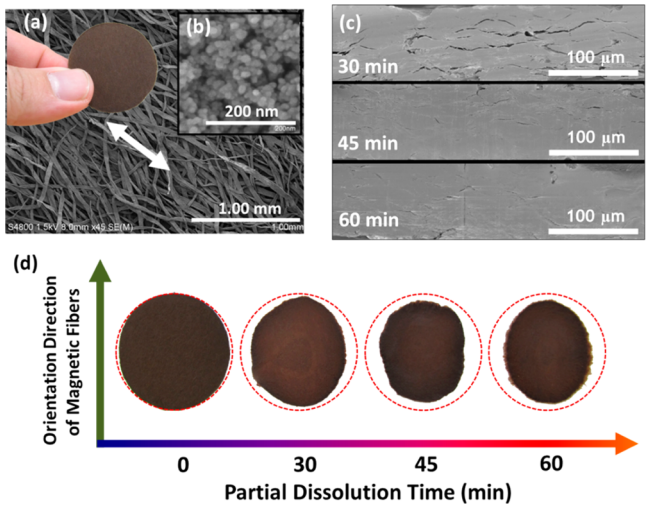

Figure 2. FE-SEM micrographs from (a) the surface of the starting unidirectional superparamagnetic fibrous mat (the double arrow shows the alignment direction), (b) the precipitated in situ synthesized magnetite nanoparticles on the surface of cellulose fibers, (c) the cross section of the produced ASPCNCs perpendicular to the alignment direction at various dissolution times. (d) Digital camera images showing the changes in the size and geometry of the produced ASPCNCs as a function of increasing partial dissolution time.

proportional to increasing the partial dissolution time, the size and shape of the resulting ASPCNCs tend to become smaller and more anisotropic, respectively. With increasing partial dissolution time, an in-plane anisotropic shrinkage perpendicular to the fibrous component direction developed.

Several parameters seem to be involved in such an observation of a considerable in-plane anisotropic shrinkage. At least part of the observation can be attributed to the filling of the structural porosities with amorphous cellulose. Amorphous cellulose acts as the matrix phase and increases the structural continuity and interactions between the fibrous components. As mentioned above, proportional to the IL-BP progress, the ratio of the amorphous cellulose to crystalline cellulose increases. During oven drying, as the last step of the IL-BISW, the matrix phase (amorphous cellulose) loses more water than the reinforcement (crystalline cellulose), leading to

dx.doi.org/10.1021/am500709t | ACS Appl. Mater. Interfaces 2014, 6, 8165−8172

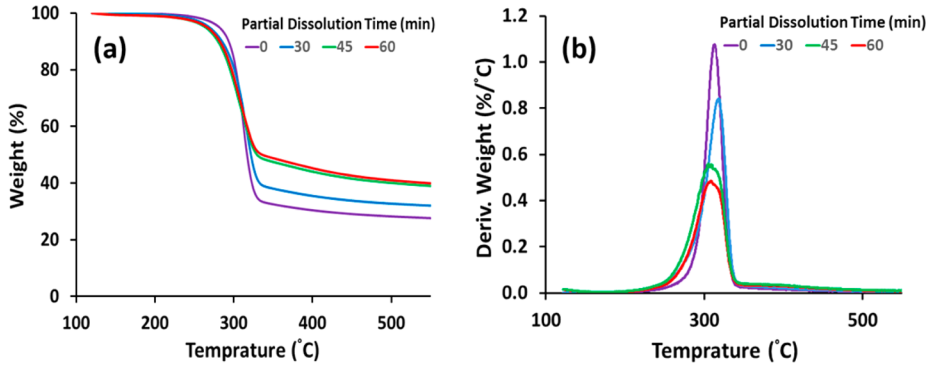

Figure 3. (a) TGA and (b) DTG curves of the superparamagnetic cellulose fiber mat and the ASPCNCs at different partial dissolution times up to 60 min (heating rate = 5 °C/min under a nitrogen atmosphere).

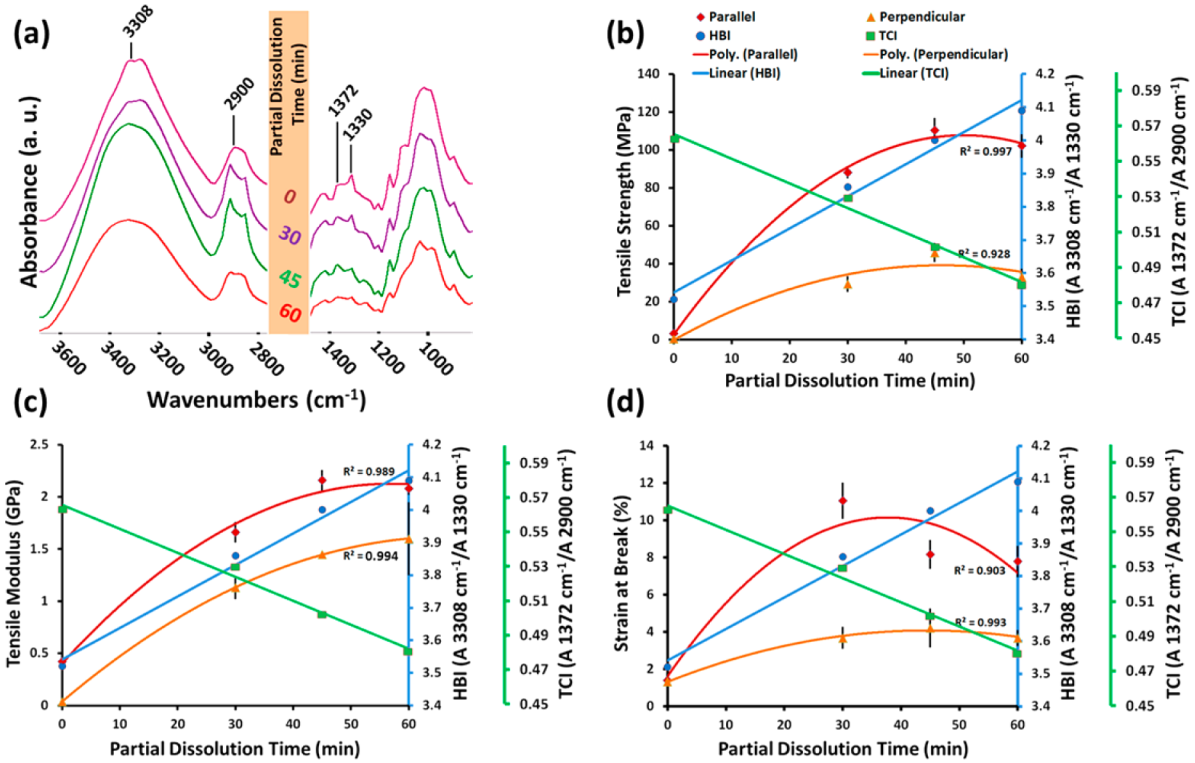

Figure 4. (a) Specific regions of ATR-FTIR spectra (between 800, 1500 and 2750, and 4000 cm^{-1}) of the USPMs and ASPCNCs. Relationships between the partial dissolution time, HBI, and TCI and (b) tensile strength, (c) tensile modulus, and (d) strain at break of the produced ASPCNCs.

more shrinkage. With increasing matrix/reinforcement ratio and better structural continuity, the effect of this shrinkage is more evident for the ASPCNCs produced at longer partial dissolution times. Also, because of the in-plane anisotropic orientation of the fibrous components and very low inherent longitudinal shrinkage of the cellulosic fibers, the intensity of the resulting in-plane shrinkage is considerably different parallel and perpendicular to the fibers. Finally, because BMIMCl mainly dissolves cellulose by breaking down the hydrogen bonds, partial dissolution might decrease the diameters of the cellulosic fibrous components more than it does their lengths.

The TGA and differential thermogravimetry (DTG) curves of the starting superparamagnetic cellulose fiber mat and produced ASPCNCs at the mentioned different partial dissolution times are presented in parts a and b of Figure 3, respectively. The results show that increasing the partial dissolution time up to 60 min slightly reduces the thermal stability because of reduction of the cellulose type I_β fraction and its substitution by amorphous cellulose. On the contrary, increasing the partial dissolution time increases the residual mass. In the case of the starting USPMs, decomposition of cellulose started around 248 °C and the maximum mass loss rate occurred at about 312 °C. With an increase in the partial dissolution time, both the starting point of decomposition and the temperature of maximum mass loss rate were slightly shifted to lower values because after a 60 min partial dissolution time these values were about 240 and 308 °C, respectively. As explained above, this is due to the increase in the amorphous cellulose fraction and its lower thermal stability than that of the cellulose type I_β.[22]

An excellent improvement in the tensile properties was observed with the IL-Process progress (Figure 4b–d). These figures also exhibit the differences between the tensile strength and Young's modulus when tested parallel and perpendicular to

dx.doi.org/10.1021/am500709t | ACS Appl. Mater. Interfaces 2014, 6, 8165–8172

the alignment direction of the fibrous components. The tensile strength and Young's modulus parallel to the direction of reinforcement were found to be 240% and 140% higher than those of the perpendicular direction, respectively. In both directions, the optimum values of the tensile properties were achieved after about 45 min of partial dissolution, so that the tensile strength parallel and perpendicular to the fibers dramatically increased about 33-fold (3300%) and 92-fold (9200%), respectively. Similarly, the Young's modulus increased about 5.2-fold (520%) and 38.2-fold (3820%) respectively for the parallel and perpendicular fiber directions. Increasing the partial dissolution time past 45−60 min reduced the mechanical properties. It seems that, up to 45 min, the amount of the cellulose type I_β that is dissolved and then resolidified is sufficient to fill all of the structural porosities and make a nanocomposites film with the optimum density. As partial dissolution progresses beyond 45 min, it can reduce the diameters of the cellulose fibers and negatively affect the mechanical properties.

Two IR ratios, A_{1372}/A_{2900} and A_{3308}/A_{1330}, were calculated to investigate the relationships between the resultant microstructural changes and tensile properties of the ASPCNCs as a function of the IL-Process progress (Figure 4a−d). The A_{1372}/A_{2900} ratio, known as the total crystallinity index (TCI),[29,30] and the A_{3308}/A_{1330} ratio, known as the hydrogen bond intensity (HBI),[31] are two very important structural parameters that have significant effects on the structural continuity and mechanical strength of the produced nanocomposite films. On the other hand, a broad peak at about 3350 cm^{-1} appears after 60 min of treatment, indicating increasing amorphous cellulose. As the results show, with increasing partial dissolution time, TCI values decreased and HBI values increased, which are indications of increased fraction of the matrix phase and improvement of the continuity and connectivity between the matrix and reinforcements.

Modeling the trend of the obtained tensile strengths showed a very good agreement with Hankinson's equation, which is well-known as a reliable 2D failure prediction model extended for predicting the fiber direction-dependent compression and tensile strengths in orthotropic wood.[32,33] In the case of the tensile strength, Hankinson's equation has the form

$$\sigma_\theta = \frac{\sigma_0\sigma_{90}}{\sigma_0 \sin^n \theta + \sigma_{90} \cos^n \theta} \quad (3)$$

where σ_θ is the ultimate tensile strength at θ degrees from the direction of the fibers and σ_0 and σ_{90} are respectively the ultimate tensile strength values parallel and perpendicular to the fibers. The exponent n can take values between 1.5 and 2 when this equation is used for predicting tensile failure.[32] Tensile strength values of the ASPCNCs prepared after 45 min of partial dissolution were experimentally obtained for three θ angles (0, 45, and 90°), and an empirical quadratic equation was obtained by curve fitting (Figure 5):

$$\sigma_\theta = 0.0049\theta^2 - 1.1611\theta + 110.33 \quad (4)$$

where σ_θ is the tensile strength (MPa).

Using this equation, the tensile strength values for the other loading angles were calculated and again curve fitting was performed. As can be seen, the trend of empirical data is in well agreement with the trend of values obtained by Hankinson's failure prediction model.

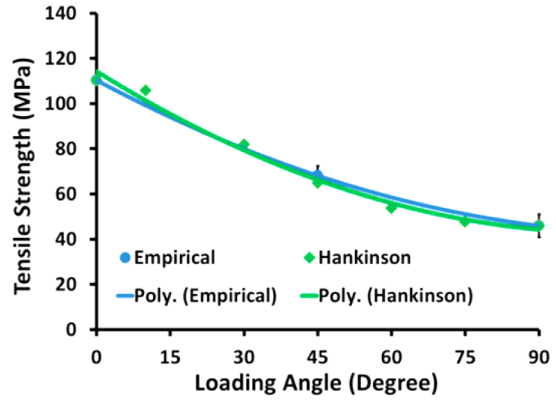

Figure 5. Relationship between the tensile strength empirical values and Hankinson's predicted values.

The effects of the IL-Process and its progress on in-plane magnetic anisotropy of the prepared samples were examined. Interestingly, it was observed that, with increasing partial dissolution time up to 60 min, the in-plane magnetic anisotropy of the resulting ASPCNCs increased about 450% (Figure 6a),

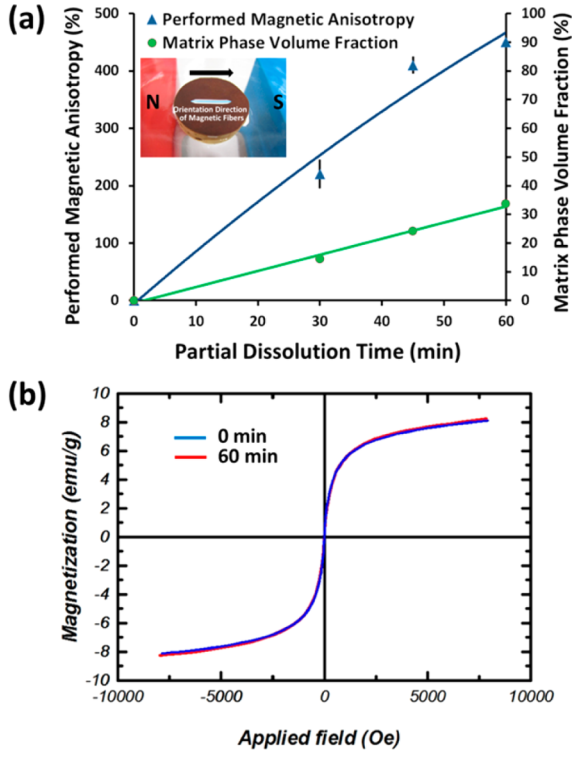

Figure 6. (a) Relationships between the partial dissolution time, matrix-phase volume fraction, and performed in-plane magnetic anisotropy of the ASPCNCs (the white line and black arrow indicate the alignment direction of fibrous components and the external modulated magnetic field direction, respectively). (b) Hysteresis loops measured for the USPM and ASPCNC films made after 60 min of partial dissolution showing superparamagnetic behavior.

while the superparamagnetic behavior remained unchanged, having the same saturation magnetization of around 8 emu/g (Figure 6b). It is known that a rise in temperature could affect the magnetic properties of magnetite nanoparticles and decrease their saturation magnetization. However, as the vibrating sample magnetometry curves show, during the IL-

dx.doi.org/10.1021/am500709t | ACS Appl. Mater. Interfaces 2014, 6, 8165−8172

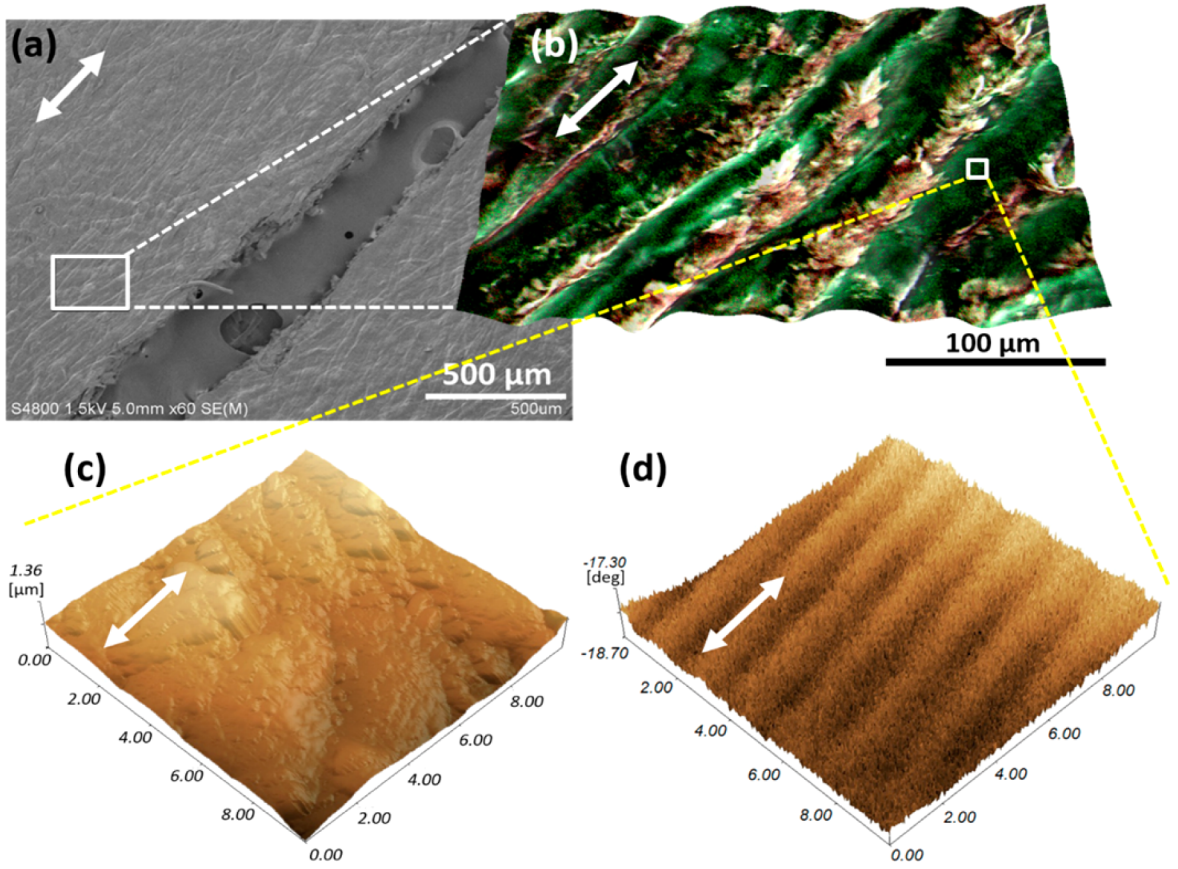

Figure 7. (a) FE-SEM micrograph from the surface of the SPCNC film made after 45 min of partial dissolution. (b) EDAX micrograph from the inscribed area in part a (the green color refers to the carbon atoms of cellulose, and the pink color refers to the iron atoms). (c) AFM and (d) MFM micrographs from a 10 × 10 μm^2 area of the surface of a partially dissolved long cellulose fiber (shown in part b). The double arrows show the modulated external magnetic field direction.

Process no change occurred in the saturation magnetization and the superparamagnetic behavior of the final ASPCNCs compared well with the initial USPMs because the maximum applied temperature during processing did not exceed 100 °C. It is confirmed that changes in the saturation magnetization of magnetite nanoparticles are remarkable when the temperature exceeds 400 °C.[34] On the other hand, these results indicate that the IL solvent, BMIMCl, has no obvious effect on the superparamagnetic properties of the magnetite nanoparticles.

To find why the magnetic anisotropy showed such significant increases with the IL-Process progress, the distribution of magnetite nanoparticles inside the structure of the ASPCNCs was investigated. Upon analysis of the obtained energy-dispersive analysis of X-rays (EDAX) maps (Figure 7b), AFM (Figure 7c), and MFM (Figure 7d), micrographs revealed some interesting facts. The EDAX maps showed that, with increasing partial dissolution time, the IL solvent peels a thicker layer off the surface of the magnetite-coated cellulose fibers and therefore a greater proportion of the cellulose matrix containing magnetite nanoparticles is formed. The gradual development of surface erosion and migration of the magnetite nanoparticles from the reinforcement surface into the matrix, on the one hand, improves the fiber−fiber interaction of the remaining partially dissolved fibrous components and, on the other hand, increases the structural and magnetic anisotropy by the formation and growth of rodlike magnetic microstructures from magnetite nanoparticles embedded in amorphous cellulose. These magnetic microstructures are formed and grow parallel to the fibrous components. Also, scanning the surface of the partially dissolved cellulose fibers using SPM revealed some other interesting facts about the reasons for improvement of the in-plane magnetic anisotropy. Parts c and d of Figure 7 were obtained using the SPM microscope from a 10 × 10 μm^2 area of the surface of a 45 min partially dissolved cellulose fiber in AFM and MFM modes, respectively. As can be seen, the surface roughness micropattern obtained by AFM is completely different from the resulting magnetic micropattern. The MFM micrographs obviously indicated the formation of a special unidirectional magnetic micropattern during the IL-BISW process.

The authors explain these observations based on the hierarchical structure of long plant cellulose fibers. Natural cellulose fibers are formed from crystalline microfibrils generally aligned along the fiber axis and bonded tightly together by noncrystalline parts. With progress of the IL-BP process, because of the different rates of partial dissolution of the crystalline and noncrystalline parts, the noncrystalline part dissolves more quickly and the resulting dissolved areas tend to trap some of the precipitated magnetite nanoparticles before they migrate to the microvoids between the fibers. This can, in turn, result in the specific magnetic pattern seen in Figure 7d. This phenomenon can subsequently affect the in-plane magnetic anisotropy of the produced ASPCNCs.

CONCLUSION

This paper reports the fabrication of a new kind of magnetocellulose nanocomposite film with engineered structure based on the all-cellulose composites concept using the IL-Process. The resulting ASPCNCs exhibit highly strong in-plane anisotropic properties structurally, mechanically, and magnetically affected by the IL-Process progress. The IL-Process significantly increased the anisotropy and strength of the produced nanocomposite films compared with the starting oriented magnetic papers. Filling the structural porosities with the amorphous cellulose and peeling off the surface of the magnetite-covered cellulose fibers resulted in improvements in the fiber−fiber interactions, on the one hand, and the formation of the magnetocellulose microrods parallel to the cellulose fibrous components and the increase in the magnetic anisotropy of each fiber, on the other hand, led to the formation of the highly in-plane anisotropic structure and superior mechanical and magnetic properties, proportional to the IL-Process progress. The highly superparamagnetic behavior of the produced nanocomposite films remained unchanged with the IL-Process progress. It is expected that the flexible and at the same time strong ASPCNCs will have a high potential for a number of advanced applications such as lightweight magnetic and flying microrobots, microswitches, and biomimetic and high-capacity information storage devices.

AUTHOR INFORMATION

Corresponding Author

*E-mail: mashkour@gau.ac.ir. Phone: +98-171-442-7050. Fax: +98-171-442-7176.

Notes

The authors declare no competing financial interest.

ACKNOWLEDGMENTS

The authors thank Dr. Ryosuke Kusumi, Dr. Arata Yushinaga, and Dr. Yoshikuni Teramoto from Kyoto University for their help with FE-SEM, EDS, and SPM.

REFERENCES

(1) Marchessault, R.; Rioux, P.; Raymond, L. Magnetic Cellulose Fibres and Paper: Preparation, Processing and Properties. *Polymer* **1992**, *33*, 4024−4028.

(2) Zakaria, S.; Ong, B.; Ahmad, S.; Abdullah, M.; Yamauchi, T. Preparation of Lumen-Loaded Kenaf Pulp with Magnetite (Fe_3O_4). *Mater. Chem. Phys.* **2005**, *89*, 216−220.

(3) Chia, C.; Zakaria, S.; Ahamd, S.; Abdullah, M.; Jani, S. M. Preparation of Magnetic Paper from Kenaf: Lumen Loading and in Situ Synthesis Method. *Am. J. Appl. Sci.* **2006**, *3*, 1750−1754.

(4) Small, A. C.; Johnston, J. H. Novel Hybrid Materials of Magnetic Nanoparticles and Cellulose Fibers. *J. Colloid Interface Sci.* **2009**, *331*, 122−126.

(5) Olsson, R. T.; Samir, M. A. S. A.; Salazar-Alvarez, G.; Belova, L.; Ström, V.; Berglund, L. A.; Ikkala, O.; Nogues, J.; Gedde, U. W. Making Flexible Magnetic Aerogels and Stiff Magnetic Nanopaper Using Cellulose Nanofibrils as Templates. *Nat. Nanotechnol.* **2010**, *5*, 584−588.

(6) Li, Y.; Zhu, H.; Gu, H.; Dai, H.; Fang, Z.; Weadock, N. J.; Guo, Z.; Hu, L. Strong Transparent Magnetic Nanopaper Prepared by Immobilization of Fe_3O_4 Nanoparticles in a Nanofibrillated Cellulose Network. *J. Mater. Chem. A* **2013**, *1*, 15278−15283.

(7) Mashkour, M.; Tajvidi, M.; Kimura, T.; Kimura, F.; Ebrahimi, G. Fabricating Unidirectional Magnetic Papers Using Permanent Magnets to Align Magnetic Nanoparticle Covered Natural Cellulose Fibers. *Bioresources* **2011**, *6*, 4731−4738.

(8) Nguyen, V. Q.; Ahmed, A. S.; Ramanujan, R. V. Morphing Soft Magnetic Composites. *Adv. Mater.* **2012**, *24*, 4041−4054.

(9) Wang, H.; Gurau, G.; Rogers, R. D. Ionic Liquid Processing of Cellulose. *Chem. Soc. Rev.* **2012**, *41*, 1519−1537.

(10) Zhang, H.; Wang, Z.; Zhang, Z.; Wu, J.; Zhang, J.; He, J. Regenerated-Cellulose/Multiwalled-Carbon-Nanotube Composite Fibers with Enhanced Mechanical Properties Prepared with the Ionic Liquid 1-Allyl-3-Methylimidazolium Chloride. *Adv. Mater.* **2007**, *19*, 698−704.

(11) Yousefi, H.; Nishino, T.; Faezipour, M.; Ebrahimi, G.; Shakeri, A. Direct Fabrication of All-Cellulose Nanocomposite from Cellulose Microfibers Using Ionic Liquid-Based Nanowelding. *Biomacromolecules* **2011**, *12*, 4080−4085.

(12) Thiemann, S.; Sachnov, S. J.; Pettersson, F.; Bollström, R.; Österbacka, R.; Wasserscheid, P.; Zaumseil, J. Cellulose-Based Ionogels for Paper Electronics. *Adv. Funct. Mater.* **2014**, *24*, 625−634.

(13) Duchemin, B. J.; Mathew, A. P.; Oksman, K. All-Cellulose Composites by Partial Dissolution in the Ionic Liquid 1-Butyl-3-Methylimidazolium Chloride. *Composites, Part A* **2009**, *40*, 2031−2037.

(14) Zhang, H.; Wu, J.; Zhang, J.; He, J. 1-Allyl-3-Methylimidazolium Chloride Room Temperature Ionic Liquid: A New and Powerful Nonderivatizing Solvent for Cellulose. *Macromolecules* **2005**, *38*, 8272−8277.

(15) Pinkert, A.; Marsh, K. N.; Pang, S.; Staiger, M. P. Ionic Liquids and Their Interaction with Cellulose. *Chem. Rev.* **2009**, *109*, 6712−6728.

(16) Nishino, T.; Matsuda, I.; Hirao, K. All-Cellulose Composite. *Macromolecules* **2004**, *37*, 7683−7687.

(17) Nishino, T.; Arimoto, N. All-Cellulose Composite Prepared by Selective Dissolving of Fiber Surface. *Biomacromolecules* **2007**, *8*, 2712−2716.

(18) Pullawan, T.; Wilkinson, A. N.; Eichhorn, S. J. Influence of Magnetic Field Alignment of Cellulose Whiskers on the Mechanics of All-Cellulose Nanocomposites. *Biomacromolecules* **2012**, *13*, 2528−2536.

(19) Duchemin, B. J.; Newman, R. H.; Staiger, M. P. Structure−Property Relationship of All-Cellulose Composites. *Compos. Sci. Technol.* **2009**, *69*, 1225−1230.

(20) Pullawan, T.; Wilkinson, A. N.; Zhang, L. N.; Eichhorn, S. J. Deformation Micromechanics of All-Cellulose Nanocomposites: Comparing Matrix and Reinforcing Components. *Carbohydr. Polym.* **2014**, *100*, 31−39.

(21) Yousefi, H.; Faezipour, M.; Nishino, T.; Shakeri, A.; Ebrahimi, G. All-Cellulose Composite and Nanocomposite Made from Partially Dissolved Micro- and Nanofibers of Canola Straw. *Polym. J.* **2011**, *43*, 559−564.

(22) Abbott, A.; Bismarck, A. Self-Reinforced Cellulose Nanocomposites. *Cellulose* **2010**, *17*, 779−791.

(23) Kim, J.; Chung, S. E.; Choi, S.-E.; Lee, H.; Kim, J.; Kwon, S. Programming Magnetic Anisotropy in Polymeric Microactuators. *Nat. Mater.* **2011**, *10*, 747−752.

(24) Boutevin, B. *Oligomers−Polymer Composites−Molecular Imprinting*; Springer: New York, 2007.

(25) Fang, W.; Panagiotopoulos, I.; Ott, F.; Boué, F.; Ait-Atmane, K.; Piquemal, J.-Y.; Viau, G.; Dalmas, F. Optimization of the Magnetic Properties of Aligned Co Nanowires/Polymer Composites for the Fabrication of Permanent Magnets. *J. Nanopart. Res.* **2014**, *16*, 1−10.

(26) Robbes, A.-S.; Cousin, F.; Meneau, F.; Dalmas, F.; Boué, F. o.; Jestin, J. Nanocomposite Materials with Controlled Anisotropic Reinforcement Triggered by Magnetic Self-Assembly. *Macromolecules* **2011**, *44*, 8858−8865.

(27) Fragouli, D.; Buonsanti, R.; Bertoni, G.; Sangregorio, C.; Innocenti, C.; Falqui, A.; Gatteschi, D.; Cozzoli, P. D.; Athanassiou, A.; Cingolani, R. Dynamical Formation of Spatially Localized Arrays of Aligned Nanowires in Plastic Films with Magnetic Anisotropy. *ACS Nano* **2010**, *4*, 1873−1878.

(28) Segal, L.; Creely, J.; Martin, A.; Conrad, C. An Empirical Method for Estimating the Degree of Crystallinity of Native Cellulose Using the X-Ray Diffractometer. *Text. Res. J.* **1959**, *29*, 786−794.
(29) Fan, M.; Dai, D.; Huang, B. Fourier Transform Infrared Spectroscopy for Natural Fibres. *Fourier Transform−Materials Analysis*; Intech: Hampshire, U.K., 2012.
(30) Nelson, M. L.; O'Connor, R. T. Relation of Certain Infrared Bands to Cellulose Crystallinity and Crystal Lattice Type. Part II. A New Infrared Ratio for Estimation of Crystallinity in Celluloses I and II. *J. Appl. Polym. Sci.* **1964**, *8*, 1325−1341.
(31) Oh, S. Y.; Yoo, D. I.; Shin, Y.; Seo, G. FTIR Analysis of Cellulose Treated with Sodium Hydroxide and Carbon Dioxide. *Carbohydr. Res.* **2005**, *340*, 417−428.
(32) Jozsef, B. *Mechanics of Wood and Wood Composites*; Van Nostrand Reinhold: New York, 1982.
(33) Kim, K. A Note on the Hankinson Formula. *Wood Fiber Sci.* **1986**, *18*, 345−348.
(34) Liu, Y.; Zhong, H.; Li, L.; Zhang, C. Temperature Dependence of Magnetic Property and Photocatalytic Activity of Fe_3O_4/Hydroxyapatite Nanoparticles. *Mater. Res. Bull.* **2010**, *45*, 2036−2039.